2014 IEEE International Conference on Robotics & Automation (ICRA)
Hong Kong Convention and Exhibition Center
May 31 - June 7, 2014. Hong Kong, China

Vision-Based Motion Control of a Flexible Robot for Surgical Applications

Alessandro Vandini, Antonino Salerno, Christopher J. Payne, Guang-Zhong Yang, *Fellow, IEEE*

***Abstract*— In recent years, continuum robots have gained significant momentum in terms of technological maturity and clinical application. Their flexibility allows complex treatment sites to be reached with minimal trauma to the patient. However the reliable control of continuum robots is still an ongoing research issue in the robotics community because their deformable structure makes the modeling of these devices difficult. This motivates the use of external sensors or vision to achieve accurate control. In this paper, a motion control framework based on a vision sensor is proposed in order to perform accurate and controlled movements of a flexible robot that is mounted to an anthropomorphic robotic arm. The vision sensor, which relies on a single camera, provides accurate 3D shape reconstruction and spatial localisation of the flexible robot. This information is used to provide feedback for the real-time control of the flexible robot. The vision sensor detects the robot first in an image stream by modeling its appearance using compressed visual features in an online learning framework. This is combined with the kinematics information from the anthropomorphic robotic arm in order to accurately reconstruct and localise the 3D shape of the flexible robot by minimizing an energy function. Detailed analysis of the framework and a validation are presented in order to demonstrate the practical value of the proposed method.**

I. INTRODUCTION

Minimally invasive surgery (MIS) has gained increasing popularity as an alternative to open surgery. It has the advantages of reduced blood loss, minimized risk of infection and shorter patient recover times. However, such surgery must be performed through small incisions in the body which makes the surgery technically challenging. One such challenge is the access constraint imposed by the incision. This problem has inspired many researchers to develop new flexible robotic tools that can navigate to the surgical site from a remote access point [1]. These designs can use articulated linkages [2], [3], [4], [5] or be of a continuum nature [6], [7], [8], [9]. Continuum-based systems can manoeuvre through smooth trajectories and tight bending radii that is an essential requirement for some MIS procedures, but their robotic control is not a trivial task because their motion is determined by smooth, continuous deformations of the robot structure than movements of rigid links and joints [10].

Continuum-based flexible robots typically used a tendon-driven approach and the modeling of these systems suffers from inaccuracies resulting from friction forces, hysteresis effects and backlash that are challenging to model [11]. These continuum systems are also sensitive to external loads that alter their kinematics [7]. This motivates the use of other external sensors to provide meaningful and reliable shape information of the robot. This shape measurement forms the input to the robot control loop, in case of vision-based shape sensing techniques, this becomes a visual servo control system [12], [13].

The use of optical fiber sensing has been investigated in the last decade in order to accurately estimate the shape of flexible devices [14], [15]. An accurate 3D shape reconstruction of a flexible needle using fiber bragg grating sensors was proposed in [16]. Optical fibre-based methods can achieve accurate measurements of the shape and are physically compact but their integration into a continuum robot is not always trivial and they can be expensive to produce.

Alternative shape sensing techniques that adopt vision-based methods are advantageous because they do not require any hardware modifications to the robot and surgical imaging equipment is already an essential component of the operating theatre. Moreover vision-based techniques can accurately measure the continuum robot shape without impeding the robots flexibility or interfering with the robot kinematics. The 3D shape reconstruction of a continuum robot based on self-organizing maps applied to stereo vision is proposed in [17]. This method does not require orthogonal cameras or fiducials applied to the body of the robot. The estimation of the pose of a continuum robot is also achieved in [10] by using learnt visual features which are robust to limited occlusions. These features are learnt offline and they link the shape configuration of the robot with its visual features. The 3D shape of a robotic catheter is reconstructed and localised using appearance priors of the catheter together with optimal C-arm rotations in [18]. In [19] the shape of the robot is calculated using a deformable surface parametrization combined with optimal viewpoints of a robotic C-arm. Although the results are promising, the method is validated only using simulated data. A fast and accurate shape estimation algorithm which models the robot deformations with circles passing through fiducials is proposed in [20]. The results obtained using the vision sensors were more precise than those estimated using internal measurements of the continuum robot; the method considers only planar motion of the robot. This approach was then extended in [11] where planes created by feature points extracted along the robot were used together with image correspondences of the robot and its forward kinematics in order to estimate the shape of the robot. This method was tested on simulated data. In [21] three orthogonal cameras are used to reconstruct the shape of a flexible manipulator using a voxel-carving approach. Although the method reaches

A. Vandini, A. Salerno, C. J. Payne and G. Z. Yang are with the Hamlyn Centre for Robotic Surgery, Imperial College London, SW7 2AZ, London, UK (e-mail: a.vandini12@imperial.ac.uk)

millimetre level accuracy, the requirement of three cameras makes it difficult to integrate into an operating room.

In this paper, a motion control framework based on a novel and robust vision sensor is proposed to allow accurate and controlled guidance of a flexible robot that is mounted to an anthropomorphic robotic arm. The vision sensor estimates the 3D shape of the flexible robot and its spatial location using only a single camera and the kinematics information derived from the anthropomorphic robotic arm. It is shown that the vision sensor is robust with inhomogeneous backgrounds. The continuous and real-time shape measurement is the input for the real-time control of the flexible robot by providing feedback of its instantaneous shape configuration. The flexible robot is first detected in an image stream by the vision sensor that models the appearance of the robot using compressed visual features in an online learning framework. The 3D shape of the flexible robot adopted for its real-time control is then reconstructed and localised by fusing the detection performed on the image to the kinematics information from the anthropomorphic robotic arm. This information fusion is performed by minimizing an energy function which mainly depends upon the distance between projections of a 3D model of the robot and its detected projection in the image, ensuring an accurate and robust estimation of the robot shape. This is then used to produce the control variable β, referred to as the bending angle, which the control system uses to control the motion of the robot. This is achieved by comparing the angle measured β with a desired bending angle β_d as shown in Sec. II.D.

Since this motion control framework is based on a vision sensor, it does not affect the flexible robot maneuverability nor is it prone to the friction, hysteresis or backlash issues seen in open-loop approaches, allowing for much greater overall accuracy of the system. Furthermore, the framework relies on a single camera which makes it easy to integrate in the clinical workflow in order to assist surgeons during minimally invasive surgery. A detailed validation of the framework was performed to illustrate its potential practical value and robustness.

The paper is structured as following: Sect. II describes the vision algorithm and the general control architecture, Sect. III presents the main results and the experimental setup used to validate the proposed framework and finally Sect. IV concludes the work with a discussion of the obtained results and directions for future works.

II. METHODS

In this section, a vision-based motion control of a flexible robot is proposed. The framework consists of: flexible robot centreline extraction, 3D shape reconstruction, control of the macro robot and control of the flexible robot. Fig. 1(a) shows a workflow of the whole proposed framework and the workflow of the vision algorithm can be found in Fig. 1(b). As shown in Fig. 1(a), the control architecture is based on the feedback loop retrieved by the estimation of the bending angle β of the flexible robot using the vision sensor. β is then compared with a desired bending angle β_d in order to

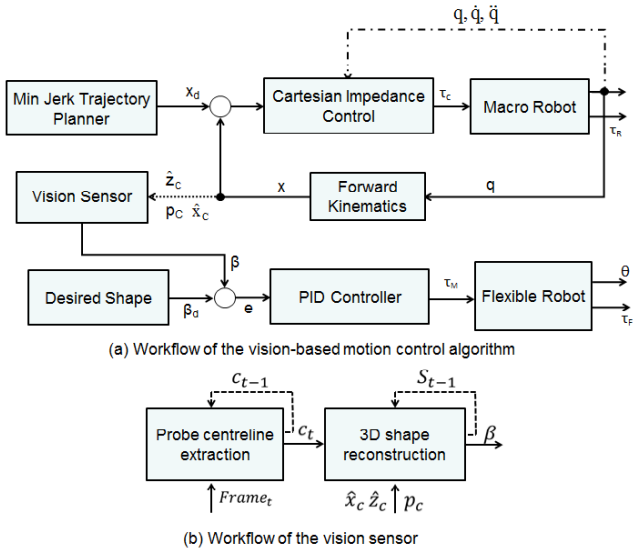

Fig. 1. In (a) the vision-based motion control algorithm of a flexible robot is shown. The workflow of the vision sensor is illustrated in (b)

produce the input command to the controller. This generates the command torques τ_M for the motion control of the flexible robot. In the following sections we will consider a flexible device with 1 degree-of-freedom (D.o.F.) mounted on the end-effector of an anthropomorphic robotic arm (with 7 D.o.F.) as the system to be controlled. The flexible section of the robot is mounted at the tip of a rigid shaft that is rigidly affixed to the macro robot. The purpose of the macro robot in Fig. 1(a), is twofold: (i) to provide the gross positioning of the flexible robot and (ii) to provide both the position of the base of the flexible section p_c and the unit vectors $\hat{x}_c$, $\hat{z}_c$ identifying the bending plane of the flexible tip to the vision algorithm.

A. Flexible Robot Centreline Extraction

The *a priori* estimation of a robust appearance model for the flexible robot is challenging due to the varying illumination conditions, deformations of the object, pose variations and occlusions. To overcome these issues, online object tracking methods can be used to learn an adaptive appearance model of the object updating it using instant observations [22]. Although these methods have shown great results, some limitations have still to be addressed such as the limited data available for the learning process and the tracking drift problem.

In our framework, a modified version of the Compressive Tracking method (CT) [22] is used to track the continuum robot. CT models the appearance of the object by compressing samples of the background and foreground with a sparse measurement matrix R. R is used to project the samples from the high-dimensional image feature space into a lower-dimensional space. These projected samples are then used as positive or negative samples of the object to train a naive Bayesian classifier online. In order to estimate the location of the object in the current frame, samples of the image are

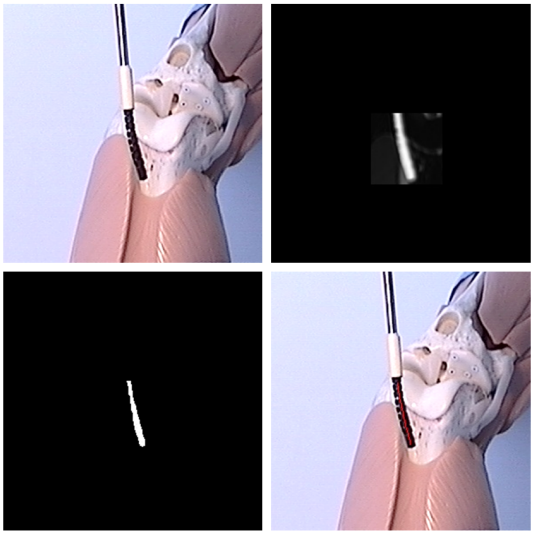

Fig. 2. An example of results from each step of the flexible robot centreline extraction is shown. In the first row the original image together with the heatmap is shown. In the second row, the flexible robot is detected and the centreline extracted (shown in red).

acquired close to the previous object location. From these samples the one that has the maximum classification score is chosen as the location of the object in the current frame.

The sampling performed in [22] that was used to train the classifier is based on a rectangle patch, also called bounding box. This patch contains the object in the case of a positive sample and the background in the case of a negative sample. In our case, the object that has to be tracked is a continuum robot which has a long thin shape as shown in Fig. 5. If only a rectangular bounding box was used to sample the robot in the image, it would contain a great area of the background. As a result, the learning of the appearance model would be negatively affected. Therefore, instead of considering the whole robot shape as our target object in the tracking framework, the robot is sampled along its body using small adjacent rectangles. Each rectangle is centred along the centreline of the robot and its size corresponds to the width of the robot shape in the image. In our framework, since the robot is described by multiple positive samples a heat map is estimated using the score of the classifier. An empirically-defined threshold is then applied to the heat map to segment the robot from the background, as shown in Fig. 2. Finally, the centreline on the flexible robot, defined as c is extracted by applying a fast thinning algorithm [23] on the segmented area belonging to the robot.

B. 3D Shape Reconstruction

The mechanical design of the flexible robot ensures its movements are restricted to a calculable plane μ, the *motion plane* which is described by two unit vectors $\hat{x}_c$ and $\hat{z}_c$. This ensures that the domain of possible solutions for the 3D shape reconstruction is limited to μ as it is shown in Fig. 3.

The shape of the continuum robot at time t is defined as

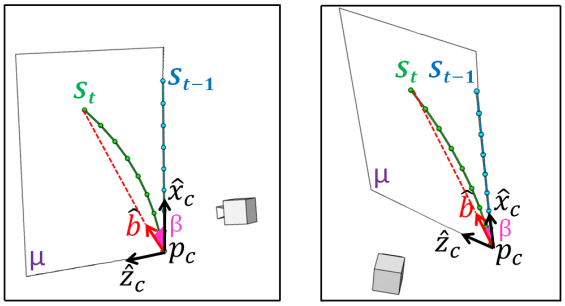

Fig. 3. The two pictures represent the same scene viewed from two different points of view. The bending angle β together with the vectors $\hat{x}_c$ and $\hat{z}_c$ that describe the motion plane μ are shown. Moreover the shapes S_{t-1} and S_t are described.

S_t and it is described as a set of equidistant 3D points. In order to estimate S_t an extended version of the algorithm proposed in [24] is used. The 3D shape of a deformable body is estimated by calculating the 3D displacements of the points of S_{t-1} that minimize the following energy function:

$$\mathbf{E}(\mathbf{u}) = \mathbf{D}(\mathbf{u}) + \alpha S_l(\mathbf{u}) + \gamma S_{\mathbf{D}}(\mathbf{u}). \quad (1)$$

$\mathbf{D}$ is the image-based difference measure between the 2D object skeleton extracted at time t and the projections of S_{t-1} displaced of $\mathbf{u}$. $\mathbf{D}$ is defined as:

$$\mathbf{D} = \frac{1}{q}\sum_{i=1}^{q} \mathbf{M}^2(\mathbf{d}(\mathbf{y_i})) \quad (2)$$

where $\mathbf{y_i}$ is the image projection of the i^{th} point of S_{t-1} after being displaced by $\mathbf{u_i}$, q is the number of points of S_{t-1}, and $\mathbf{M}$ is the distance map estimated using the 2D object skeleton. $S_{\mathbf{D}}$ is the smoothness term and S_l is the length preserving term [24]. The coefficients α and γ are weights and were empirically chosen to be 4 and 0.2, respectively.

In [24], the recovery of the 3D shape is performed using multiple views and allowing the displacement of the points that compose the shape in the entire 3D space. Although only a single view is available in our case, it is known that the shape of the flexible robot lies on μ. Therefore $\mathbf{u}$ can be defined in term of $\hat{x}_c$ and $\hat{z}_c$ as $\mathbf{u} = \hat{x}_c\mathbf{z_x} + \hat{z}_c\mathbf{z_y}$, where $\mathbf{z} = (\mathbf{z_x}, \mathbf{z_y})$ is the displacement of S_{t-1} on μ. This restricts the space of solutions to μ and decreases the number of unknowns from $3q$ to $2q$.

In our case the 2D object skeleton calculated at time t is c_t, namely the centreline of the flexible robot. Moreover, since a 2D to 3D correspondence between c_t and S_{t-1} is known, the distances of the projections of the displaced endpoints of S_{t-1} used to find $\mathbf{D}$ are calculated considering the endpoints of the c_t instead of $\mathbf{M}$.

The estimated S_t is used to calculate the bending angle β which is the angle between the unit vector $\hat{x}_c$ and the unit vector $\hat{b}$. $\hat{b}$ is defined as the directional vector that describes the line that connects the base of the flexible robot section p_c with the tip of the flexible robot, namely the last point of S_t, as shown in Fig. 3.

C. Control of the Macro Robot

In order to guarantee a safe human robot interaction during surgery, the Cartesian impedance control has been chosen as the controller of the macro robot since it performs the gross positioning of the flexible robot *in situ*. The impedance control law can be found in details in [25] and [26].

The control law can be expressed as

$$\tau_c = J^T(q)K\left(x_d - x(q)\right) + D(d_c) + F_d(q, \dot{q}, \ddot{q}) \tag{3}$$

where, $J(q) \in \Re^{6\times n}$ is the Jacobian matrix depending on the configuration q for a robot with n joints, $K \in \Re^{6\times n}$ is a diagonal stiffness matrix, $x = [p \quad \varphi]^T$ is the actual pose in terms of position p and orientation φ, $D(d_c)$ is a damping vector depending on the damping coefficients d_c and $F_d(q, \dot{q}, \ddot{q})$ is the robot dynamics compensation including the terms of the inertia matrix, centrifugal and Coriolis torques, friction and the gravitational torque vector. The vectors of joints position, velocity and acceleration are $q, \dot{q}, \ddot{q}$, respectively. The desired pose x_d for the gross positioning of the flexible robot has been computed by means of a minimum jerk trajectory planner relying on a fifth order polynomial function as arch length [27], [28]. The vision-based control system of the flexible robot controls the fine tip placement.

The main benefit of the above control approach is that the robot's visco-elastic properties during interaction with the patient's tissue can be regulated by tuning the robot stiffness K and damping the D matrices according to the robot behaviour like a passive mass-spring-damper system.

With reference to Fig. 4, the pose vector x of the tool frame $\{C\}$ with respect to the base frame $\{B\}$ can be retrieved by the forward kinematics in terms of the following homogeneous transformation matrix:

$$T_c^b(q) = \begin{bmatrix} R_c^b & p_c^b \\ 0^T & 1 \end{bmatrix} \tag{4}$$

where $R_c^b \in SO(3)$ and p_c^b are respectively the rotation matrix and origin position of the tool frame $\{C\}$ with respect to the base frame $\{B\}$. As shown in Fig. 4, the reference frame $\{C\}$ is placed at the beginning of the flexible tip and the structure can be considered with rigid links and rigid joints up to the point C, thus the position p_c^b and the unitary vectors $\hat{x}_c$, $\hat{z}_c$ provide the input for the shape computation of the flexible tip. $\hat{x}_c$ and $\hat{z}_c$ are respectively the first and the third column of the rotation matrix R_c^b.

D. Control of the Flexible Robot

To guarantee high disturbance rejection and enhanced trajectory tracking capabilities, a decentralized control structure has been adopted to control the motion of the flexible tip [29].

The command torque τ_M at motor level can be summarized as

$$\tau_M = K_P e + K_D \dot{e} + K_I \int e(t)dt \tag{5}$$

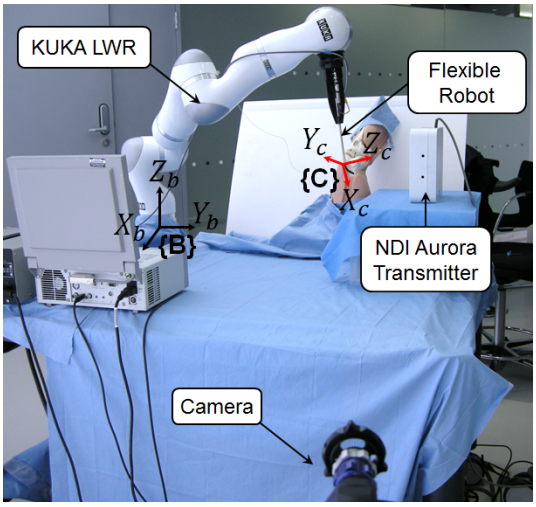

Fig. 4. Experimental setup with main components and reference frames placement.

where $e = (\theta_d - \theta)$ is the error signal between the desired angular position θ_d and the actual angular position θ of the motor, K_P, K_D and K_I are respectively the position, velocity and integral constants.

Extensive explanation about the control gains in eq. (5), the transfer function, frequency response and disturbance rejection factor of the PID controller can be found in [29].

The desired motor velocity $\dot{\theta}_d$ (and consequently the position θ_d) can be controlled as

$$\dot{\theta}_d = \begin{cases} \dot{\theta}_N & \text{if } \beta \leq (\beta_d - h) \\ -\dot{\theta}_N & \text{if } \beta \geq (\beta_d + h) \\ 0 & \text{if } (\beta_d - h) < \beta < (\beta_d + h) \end{cases}$$

where $\dot{\theta}_N$ is the nominal velocity of the motor in order to guarantee continuous operation during surgery. β_d, which is the desired angle, is related to the desired shape to be reached by the flexible tip and β is calculated on the current shape reconstructed by the vision algorithm in Sect. II.B. The parameter h acts as threshold which can be tuned according to the accuracy required and the surgical task to be performed.

E. The Flexible Robot

The robotic device, which is shown in Fig. 5, incorporates a profiled flexible probe. The probe tip can be deflected using an antagonistic tendon system; it extends the design initially presented in [30]. The probe is manufactured from superelastic Nitinol ASTM F 2063 using wire-based electro discharge machining (EDM) to allow large deflections. The design is intended to have flexibility in a single plane and adopts a machined profile that ensures stiffness in the plane orthogonal to bending through the use of a spine of 0.3mm in width. This spine also gives the probe axial rigidity which prevents de-tensioning of the tendons during operation which can lead to hysteresis effects. Stress-relieving fillet features are incorporated to prevent high stresses in the bending

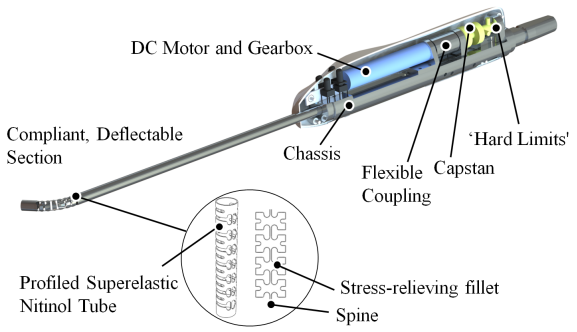

Fig. 5. Design of the flexible robot.

regions which can lead to fracture and low fatigue strength. A series of nitinol guides have been fabricated into the profile of the design to allow the tendons to be routed through. The tendons terminate at the instrument tip and are routed back to a pulley system that allows a central channel to be passed through the bore of the instrument. The tendons are affixed to a rotatable capstan mechanism in the proximal actuation system which is coupled to a DC motor with position encoding (1226 A 012 BK1855, Faulhaber) and incorporating a 256:1 ratio gearbox (256:1 12/4, Faulhaber). Hard position limits have also be incorporated to prevent overloading of the flexible probe.

III. EXPERIMENTS AND RESULTS

A. Experimental Setup

The experimental setup consists of the custom-made flexible instrument attached to the end-effector of a KUKA Lightweight Robotv 4+ (i.e. LWR), a Storz Tele Pack light box endowed with a camera, a NDI Aurora tracking system and a knee phantom as shown in Fig. 4.

The Lightweight Robot 4+ (KUKA Roboter GmbH, Augsburg, Germany) is a robotic manipulator. It has 7 revolute joints *i.e.* 7-D.o.F., a load-to-weight ratio of approximately 1:1, a tip velocity of $6\,m/s$, a workspace of up to $1.5\,m^3$ and high dynamic performance suitable for interaction with human tissue. Further details can be found in [26]. The flexible instrument is extensively described in Sect. II.E. The selected angular velocity of the motor shaft is 0.0016 rad/s.

The NDI Aurora is an electromagnetic measurement system designed specifically to track the position and shape of surgical tools and instruments such as needles, catheters, probes, and scopes. Its accuracy is 0.48 mm and 0.30 deg for position and orientation measurements respectively. The Aurora system has been used to validate the vision algorithm by through integration of the Aurora receiver in to the tip of the flexible robot. The robustness of the Aurora sensor to electromagnetic distortions has been empirically tested. Known movements of the sensor have been performed using the KUKA LWR. At each movement a measurement of the electromagnetic sensor has been acquired and compared to the motion information obtained by the KUKA LWR. No relevant distortions of the sensor have been measured compared to its nominal accuracy.

Both control of KUKA LWR and vision-based control of the flexible instrument run in a desktop PC with the following features: i7-2600 at 3.40 GHz, 16 GB of RAM and Windows 7 as operating system. The KUKA LWR, flexible instrument, camera and Aurora have been synchronized in the main control program written in C++. It is a multi-threaded program and is capable of running both the control of the KUKA LWR at 200 Hz and the vision-based control of the flexible device at about 3 Hz in parallel. 0.14 s and 0.22 s are the mean computation time for the centreline extraction and for the 3D shape reconstruction, respectively. The total computation time is 0.36 s with an unoptimized C++ implementation.

In order to evaluate the performance of the vision sensor and the control algorithm, six different positions of the KUKA LWR workspace have been chosen. The algorithm has been tested using a white board as a background for four positions and a phantom knee as background for the remaining two. The positions have been selected in order to test the vision algorithm when the flexible robot bending plane, namely the *motion plane* μ, was out-of-plane with respect to the camera. A calibration between the coordinate system of the camera, the KUKA LWR and the Aurora was performed in order to map the coordinate systems of all the devices in the coordinate system of the KUKA LWR.

A point-to-point motion [29] based on a minimum jerk arch length has been performed to reach such positions of the KUKA LWR workspace. The axis/angle technique [29] has been used to plan the orientation of the robot end-effector and of the flexible instrument. For each trial, the robotic arm was commanded to move to a position (with accuracy $0.1\,mm$, as declared by the manufacturer) before the flexible robot end-effector was actuated.

For each position of the robot end-effector, the control loop performance was evaluated for a range of desired bending angles in which β_d was chosen to be $10°$, $20°$ and $30°$, starting from an approximate straight configuration of the flexible robot. The error in the estimation of β by the vision sensor is calculated as an absolute value of the difference between the angle calculate using the tip position acquired using the Aurora and the angle calculated using tip of the shape estimated by the vision sensor. The tip error is estimated by calculating the Euclidean distance between the tip position provided by the Aurora and the tip of the shape calculated using the vision sensor. For each position the centreline extraction algorithm was manually initialised providing the centreline of the flexible robot on the first frame. Moreover the initial 3D shape used for the 3D shape reconstruction was chosen to be a straight segment with the same length of the flexible robot, located on p_c and having the same direction of $\hat{x}_c$. For all the experiments the threshold h was set to $2°$.

B. Results

In Fig. 6(a) the angle β estimated by the vision sensor (VS angle) and the angle calculated using the Aurora (EM angle) during the first trial using the knee phantom are shown. The

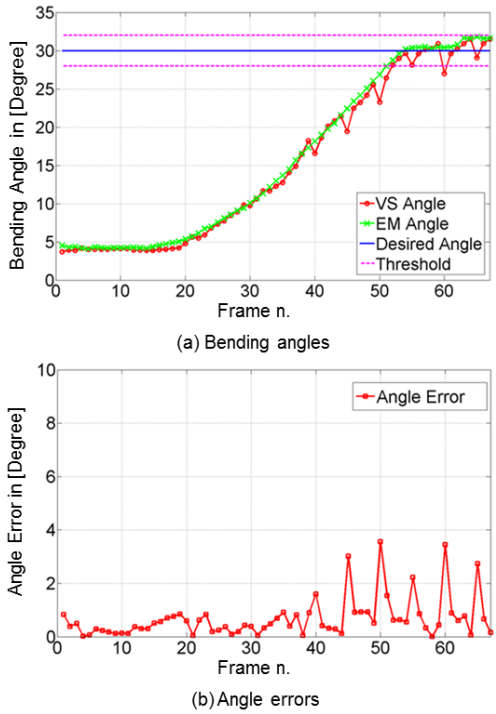

Fig. 6. The bending angle calculated using the Aurora system (EM angle) and the vision sensor (VS angle) is reported in (a) for the first position of KUKA LWR using the knee. The control starts at 10th frame and the desired angle is 30°. In (b) for the same position of (a) the angle errors which are calculated as the absolute value of the difference between VS angle and EM angle are reported.

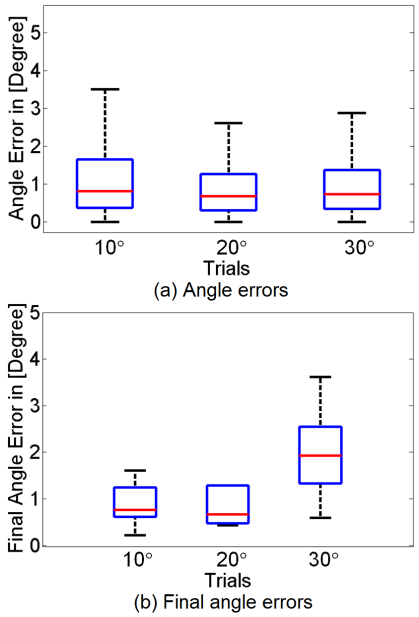

Fig. 7. The angle errors calculated for each frame of all the trials grouped by the desired angle are shown in (a). In (b) are shown the final angle errors, namely the difference between the measurement acquired at the end of the trial and the desired angle, for all the trials performed grouped by desired angle.

frames reported on the axis represent the frame processed by the vision algorithm. The control task starts at the 10th frame. The angle errors for each frame of the same trial are reported in Fig. 6(b). The vision sensor is able to provide a reliable and precise bending angle with respect to the Aurora sensor as it shown in Fig. 6(b). Moreover, from Fig. 6(a) it is possible to observe that the control of the flexible robot converges to the desired angle β_d.

The angle errors calculated for each frame of all the trials grouped by the desired angle are shown in Fig. 7(a). The mean value of the error angle is below 1°. The Fig. 7(b) shows the final angle errors, namely the difference between the measurement acquired at the end of the trial and the desired angle, for all the trials performed grouped by desired angle. These results demonstrate that the algorithm converges at the desired angle with good accuracy.

A summary of the performance of the vision sensor is shown in Table I where the angle errors calculated for each frame of all the trials are grouped by the position of the KUKA LWR.

The vision sensor reaches an accuracy of approximately 1° on the bending angle of the flexible robot and about 1/2 mm on the localisation of the tip. Moreover it is possible to observe in Fig. 6 and in Table I that the errors are not affected by employing a non-homogeneous background such as the knee phantom. The highest mean value of the error shows in Table I is from the trial number 4 where the motion plane μ was about 45° out-of-plane of the camera. This means that although the motion of the flexible robot was out-of-plane of the camera, the algorithm was still able to perform with good accuracy in limiting the localisation and reconstruction errors.

TABLE I

3D LOCALISATION ERRORS IN [MM] FOR THE TIP OF THE FLEXIBLE ROBOT AND ANGLE ERRORS IN [DEGREE] FOR THE EXPERIMENTS CONDUCTED WITH A WHITE BOARD AND WITH A PHANTOM KNEE.

	White Board				**Knee**	
Positions	1	2	3	4	1	2
Mean Tip	1.43	2.98	1.07	2.08	2.23	1.27
StdDev Tip	0.34	0.81	0.89	1.00	0.47	0.63
Mean Angle	1.03	0.95	0.86	1.30	1.02	0.71
StdDev Angle	0.67	0.88	0.88	1.07	0.92	0.59

IV. CONCLUSIONS

In this work, a vision-based motion control framework of a flexible robot for surgical applications is proposed. The novel and robust vision sensor provides accurate and online shape measurements of the flexible robot that feeds its control unit. The framework is based on a single camera and from position information acquired from an anthropomorphic robotic arm where the flexible robot is attached. The results demonstrate the overall robustness of the framework which is able to converge to the desired angle purely by the images acquired from a single camera. Such a configuration is easily satisfied in MIS as an additional endoscope is usually deployed along with the surgical instrumentation. The vision sensor is able to provide fast and accurate measurement of the shape also in

the presence of a non-homogeneous background. Moreover it reaches millimeters accuracy on the detections of the tip. Finally, the shape of the flexible robot is continuously estimated without the addition or integration of expensive and bothersome new hardware in to the flexible robot.

The integration of the vision-based control with dynamic active constraints and virtual fixtures [31] is envisaged as a further application of the proposed algorithm in order to achieve hands-on cooperative control. In this scenario, the surgeon shares control of the surgical instrument with the macro robot in which software constraints are applied to the flexible tool motion in order (i) to guide the instrument to the target anatomy *in situ*, thus avoiding collisions with surrounding healthy tissues; (ii) to provide the haptic feedback to the surgeon; (iii) to autonomously control the flexible instrument with the purpose of increasing the surgeons dexterity and to reduce the number of D.o.F.s that the surgeon has to directly control. Moreover a study on the optimal configurations of the bending plane of the flexible robot considering the point of view of the camera will be performed.

ACKNOWLEDGMENT

The authors would like to thank Dr Stamatia Giannarou, Konrad Leibrandt and Petros Giataganas for their contributions to this research. This work was supported by the Wellcome Trust and the Engineering and Physical Sciences Research Council as part of the Medical Engineering Solutions in Osteoarthritis Centre of Excellence [088844/Z/09/Z] project.

REFERENCES

[1] V. Vitiello, S. Lee, T. Cundy, G. Yang, "Emerging robotic platforms for minimally invasive surgery." *IEEE Reviews in Biomedical Engineering*, vol. 6, pp. 111–126, 2013.

[2] J. Shang, D. P. Noonan, C. Payne, *et al.*, "An articulated universal joint based flexible access robot for minimally invasive surgery," in *IEEE International Conference on Robotics and Automation*, 2011, pp. 1147–1152.

[3] J. Shang, C. J. Payne, J. Clark, *et al.*, "Design of a multitasking robotic platform with flexible arms and articulated head for minimally invasive surgery," in *IEEE/RSJ International Conference on Intelligent Robots and Systems*, 2012, pp. 1988–1993.

[4] A. Degani, H. Choset, A. Wolf, and M. Zenati, "Highly articulated robotic probe for minimally invasive surgery," in *IEEE International Conference on Robotics and Automation*, 2006, pp. 4167–4172.

[5] G. Petroni, M. Niccolini, A. Menciassi, *et al.*, "A novel intracorporeal assembling robotic system for single-port laparoscopic surgery," *Surgical endoscopy*, pp. 1–6, 2012.

[6] N. Simaan, K. Xu, W. Wei, *et al.*, "Design and integration of a telerobotic system for minimally invasive surgery of the throat," *The International journal of robotics research*, vol. 28, no. 9, pp. 1134–1153, 2009.

[7] D. Camarillo, C. Milne, C. Carlson, *et al.*, "Mechanics modeling of tendon-driven continuum manipulators," *IEEE Transactions on Robotics,*, vol. 24, no. 6, pp. 1262–1273, 2008.

[8] M. Kutzer, S. Segreti, C. Brown, *et al.*, "Design of a new cable-driven manipulator with a large open lumen: Preliminary applications in the minimally-invasive removal of osteolysis," in *IEEE International Conference on Robotics and Automation*, 2011, pp. 2913–2920.

[9] J. Ding, K. Xu, R. Goldman, *et al.*, "Design, simulation and evaluation of kinematic alternatives for insertable robotic effectors platforms in single port access surgery," in *IEEE International Conference on Robotics and Automation*, 2010, pp. 1053–1058.

[10] A. Reiter, R. E. Goldman, A. Bajo, *et al.*, "A learning algorithm for visual pose estimation of continuum robots," in *International Conference on Intelligent Robots and Systems*, 2011, pp. 2390–2396.

[11] V. Chitrakaran, A. Behal, D. Dawson, and I. Walker, "Setpoint regulation of continuum robots using a fixed camera," *Robotica*, vol. 25, no. 5, pp. 581–586, 2007.

[12] F. Chaumette and S. Hutchinson, "Visual servo control. i. basic approaches," *IEEE Robotics Automation Magazine*, vol. 13, no. 4, pp. 82–90, Dec 2006.

[13] S. Hutchinson, G. Hager, and P. Corke, "A tutorial on visual servo control," *IEEE Transactions on Robotics and Automation*, vol. 12, no. 5, pp. 651–670, Oct 1996.

[14] R. Posey Jr, G. Johnson, and S. Vohra, "Strain sensing based on coherent rayleigh scattering in an optical fibre," *Electronics Letters*, vol. 36, no. 20, pp. 1688–1689, 2000.

[15] Y.-L. Park, K. Chau, R. J. Black, *et al.*, "Force sensing robot fingers using embedded fiber bragg grating sensors and shape deposition manufacturing," in *IEEE International Conference on Robotics and Automation*, 2007, pp. 1510–1516.

[16] M. K. Momen Abayazid and S. Misra, "3d flexible needle steering in soft-tissue phantoms using fiber bragg grating sensors," in *IEEE International Conference on Robotics and Automation*, 2013, pp. 5823–5829.

[17] J. M. Croom, D. C. Rucker, J. M. Romano, *et al.*, "Visual sensing of continuum robot shape using self-organizing maps," in *IEEE International Conference on Robotics and Automation*, 2010, pp. 4591–4596.

[18] A. Vandini, S. Giannarou, S.-L. Lee, and G.-Z. Yang, "3D robotic catheter shape reconstruction and localisation using appearance priors and adaptive c-arm positioning," in *MIAR 2013*, ser. LNCS, vol. 8090. Berlin, Heidelberg: Springer-Verlag, 2013.

[19] E. J. Lobaton, J. Fu, L. G. Torres, *et al.* "Continuous shape estimation of continuum robots using x-ray images," in *IEEE International Conference on Robotics and Automation*, 2013, pp. 717–724.

[20] M. W. Hannan and I. D. Walker, "Real-time shape estimation for continuum robots using vision," *Robotica*, vol. 23, no. 05, pp. 645–651, 2005.

[21] D. B. Camarillo, K. E. Loewke, C. R. Carlson, and J. K. Salisbury, "Vision based 3-d shape sensing of flexible manipulators," in *IEEE International Conference on Robotics and Automation*, 2008, pp. 2940–2947.

[22] K. Zhang, L. Zhang, and M.-H. Yang, "Real-time compressive tracking," in *European Conference on Computer Vision*. Springer, 2012, pp. 864–877.

[23] T. Zhang and C. Y. Suen, "A fast parallel algorithm for thinning digital patterns," *Communications of the ACM*, vol. 27, no. 3, pp. 236–239, 1984.

[24] R. Liao, Y. Tan, H. Sundar, and et al., "An efficient graph-based deformable 2D/3D registration algorithm with applications for abdominal aortic aneurysm interventions," in *MIAR 2010*, ser. LNCS, vol. 6326. Berlin, Heidelberg: Springer-Verlag, 2010, pp. 561–570.

[25] A. Albu-Schäffer, C. Ott, and G. Hirzinger, "A unified passivity-based control framework for position, torque and impedance control of flexible joint robots," *The International Journal of Robotics Research*, vol. 26, no. 1, pp. 23–39, 2007.

[26] A. Albu-Schäffer, S. Haddadin, C. Ott, *et al.*, "The dlr lightweight robot: design and control concepts for robots in human environments," *Industrial Robot: An International Journal*, vol. 34, no. 5, pp. 376–385, 2007.

[27] K. Kyriakopoulos and G. Saridis, "Minimum jerk path generation," in *IEEE International Conference on Robotics and Automation*, 1988, pp. 364–369 vol.1.

[28] L. Zollo, A. Salerno, L. Rossini, and E. Guglielmelli, "Submovement composition for motion and interaction control of a robot manipulator," in *IEEE RAS and EMBS International Conference on Biomedical Robotics and Biomechatronics (BioRob)*, 2010, pp. 46–51.

[29] B. Siciliano, L. Sciavicco, L. Villani, and G. Oriolo, "Robotics: Modelling, planning and control," 2008.

[30] E. Lopez, K.-W. Kwok, C. J. Payne, *et al.*, "Implicit active constraints for robot-assisted arthroscopy," in *IEEE International Conference on Robotics and Automation*, 2013, pp. 5370–5375.

[31] K.-W. Kwok, K. H. Tsoi, V. Vitiello, *et al.*, "Dimensionality reduction in controlling articulated snake robot for endoscopy under dynamic active constraints," *IEEE Transactions on Robotics,*, vol. 29, no. 1, pp. 15–31, 2013.